Characterization in Mice of the Resident Mesenchymal Niche Maintaining At2 Stem Cell Proliferation in Homeostasis and Disease

Sara Taghizadeh, Monika Heiner, Ana Ivonne Vazquez-Armendariz, Jochen Wilhelm, Susanne Herold, Chengshui Chen, Jin San Zhang, Saverio Bellusci

TISSUE-SPECIFIC STEM CELLS

STEM CELLS®

Characterization in mice of the resident mesenchymal niche maintaining AT2 stem cell proliferation in homeostasis and disease

Sara Taghizadeh[1,2] | Monika Heiner[2] | Ana Ivonne Vazquez-Armendariz[3] |
Jochen Wilhelm[2,3] | Susanne Herold[2] | Chengshui Chen[1] | Jin San Zhang[1] |
Saverio Bellusci[1,2] [ID]

[1]Department of Pulmonary and Critical Care Medicine, Key Laboratory of Interventional Pulmonology of Zhejiang Province, The First Affiliated Hospital of Wenzhou Medical University, Wenzhou

[2]Department of Pulmonary and Critical Care Medicine and Infectious Diseases, Cardio-Pulmonary Institute, Universities of Giessen and Marburg Lung Center (UGMLC), Member of the German Center for Lung Research (DZL), Justus-Liebig University Giessen, Germany

[3]Institute for Lung Health (ILH), Germany

Correspondence
Jin San Zhang, MD, Key Laboratory of Interventional Pulmonology of Zhejiang Province, Department of Pulmonary and Critical Care Medicine, The First Affiliated Hospital of Wenzhou Medical University, Wenzhou 325035, People's Republic of China.
Email: zhang_jinsan@wmu.edu.cn

Saverio Bellusci, PhD, Department of Pulmonary and Critical Care Medicine and Infectious Diseases, Cardio-Pulmonary Institute, Universities of Giessen and Marburg Lung Center (UGMLC), Member of the German Center for Lung Research (DZL), Justus-Liebig University Giessen, Giessen, Germany.
Email: saverio.bellusci@innere.med.uni-giessen.de

Abstract

Resident mesenchymal cells (rMCs defined as Cd31^{Neg}Cd45^{Neg}Epcam^{Neg}) control the proliferation and differentiation of alveolar epithelial type 2 (AT2) stem cells in vitro. The identity of these rMCs is still elusive. Among them, Axin2^{Pos} mesenchymal alveolar niche cells (MANCs), which are expressing *Fgf7*, have been previously described. We propose that an additional population of rMCs, expressing *Fgf10* (called rMC-Sca1^{Pos}Fgf10^{Pos}) are equally important to maintain AT2 stem cell proliferation. The alveolosphere model, based on the AT2-rMC co-culture in growth factor-reduced Matrigel, was used to test the efficiency of different rMC subpopulations isolated by FACS from adult murine lung to sustain the proliferation and differentiation of AT2 stem cells. We demonstrate that rMC-Sca1^{Pos}Fgf10^{Pos} cells are efficient to promote the proliferation and differentiation of AT2 stem cells. Co-staining of adult lung for *Fgf10* mRNA and Sftpc protein respectively, indicate that 28% of Fgf10^{Pos} cells are located close to AT2 cells. Co-ISH for *Fgf7* and *Fgf10* indicate that these two populations do not significantly overlap. Gene arrays comparing rMC-Sca1^{Pos}Axin2^{Pos} and rMC-Sca1^{Pos}Fgf10^{Pos} support that these two cell subsets express differential markers. In addition, rMC function is decreased in obese *ob/ob* mutant compared to WT mice with a much stronger loss of function in males compared to females. In conclusion, rMC-Sca1^{Pos}Fgf10^{Pos} cells play important role in supporting AT2 stem cells proliferation and differentiation. This result sheds a new light on the subpopulations of rMCs contributing to the AT2 stem cell niche in homeostasis and in the context of pre-existing metabolic diseases.

Significance statement

The characterization of the resident mesenchymal cells (rMC) in the lung capable of sustaining the proliferation and differentiation of AT2 stem cells is paramount to design therapeutic strategies aiming at restoring the AT2 pool after massive injury. Using the alveolosphere AT2-rMC co-culture model, this study identified, for the first time, rMC-Sca1^{Pos}Fgf10^{Pos}-LIFs as displaying this critical niche activity. In addition, using the ob/ob mice, the niche activity of rMC-Sca1^{Pos} cells was shown to be negatively impacted by gender and obesity. The authors propose that rMC deficiency could be causative for the acute lung injury and fibrosis observed in male and obese patients suffering from COVID-19.

1 | INTRODUCTION

Lung fibrosis is characterized by an accumulation in the respiratory airways of mesenchymal cells, called activated myofibroblasts (MYF) which over time, lead to impaired lung function.[1] Through the use of single cell transcriptomic approach, the heterogeneity of the different resident mesenchymal (rMC) populations present in the lung is starting to emerge. A key stromal cell is represented by the lipofibroblasts (LIFs), which are rich in lipid-droplets and can be stained and isolated using the vital dye LipidTox (LT). They express $Perilipin\ 2$, $Platelet\ derived\ growth\ factor\ receptor\ alpha$ ($Pdgfra$) and are negative for Acta2 and most importantly are located close to alveolar type 2 cells (AT2).[2] They are proposed to supply AT2s with the triglycerides needed for the elaboration of surfactant. Using a co-culture assay of Pdgfrα^{High} mesenchymal cells and AT2s in growth factor-reduced Matrigel, it has been proposed that the rMC-LIFs are essential for the maintenance of the proliferation and differentiation of AT2 stem cells.[3]

$Fibroblast\ growth\ factor\ 10$ ($Fgf10$) is a mesenchymal-specific gene expressed in the distal part of the embryonic lung during the early pseudoglandular stage.[4] Our lineage tracing analyses have shown that a subpopulation of Fgf10^{Pos} cells at embryonic day 12.5 serves as progenitor for rMC-LIFs at later stages of lung development.[5] Additionally, in postnatal lungs, around 30% of rMC-LIF express the $Fgf10$ gene.[2] The relevance of these rMC-Fgf10^{Pos} LIF in maintaining the proliferation and differentiation of AT2 stem cells remains to be demonstrated. Interestingly, another population of stromal cells, called MANC (Mesenchymal Alveolar Niche Cells), which are positive for $Axin2$, $Pdgfra$, $Wnt2$, $Il6$ and $Fgf7$,[6] were also described to locate close to AT2 cells. How different are the rMC-Fgf10^{Pos} LIFs to the MANC is still unclear.

Using lineage tracing, we previously reported the reversible transdifferentiation of the LIFs into activated MYF during fibrosis formation and resolution.[7] In addition, Metformin, a first line antidiabetic drug has been reported to enhance the activated MYF to LIF transition both in vitro and in vivo.[8] Repetitive damages to AT2s have been proposed to be linked to the development of lung fibrosis.[9] Interestingly, one of the major and long-term complication for patients who survived SARS-CoV-2 infection (leading to COVID-19 disease) is fibrosis.[10,11] SARS-CoV-2 binds to its receptor angiotensin converting enzyme II (ACEII) mostly abundantly expressed in the AT2s. Massive damages to the AT2s likely unleashes the associated LIFs to become activated MYFs, thereby leading to fibrosis. Pertinent to this background, obesity/diabetes and gender have been proposed to be predictive factors for the severity of the disease.[12,13]

In this study, we used the in vitro alveolosphere model based on the AT2-rMC co-culture in growth factor-reduced Matrigel to test the efficiency of different rMC subpopulations isolated by FACS from adult murine lung. We used antibodies against Cd45, Cd31, Epcam and Stem cell antigen 1 (Sca1) to refine the initial rMC population responsible for the proliferation of AT2 stem cells. Using a fluorescent substrate for ß-galactosidase activity, rMC-Sca1^{Pos}Fgf10^{Pos} as well as rMC-Sca1^{Pos}Axin2^{Pos} cells were sorted. Additional sorting was achieved using LipidTOX (LT) staining for cells containing high level of neutral lipids. After 2 weeks of co-culture, organoid size and colony forming efficiency were quantified. RNAscope with $Fgf7$- and $Fgf10$-labeled riboprobes, to label rMC-Axin2^{Pos} and rMC-Fgf10^{Pos} respectively, combined with Sftpc immunofluorescence on adult lungs was carried out. Gene array analyses were used to characterize sorted rMC-Sca1^{Pos}Fgf10^{Pos} vs rMC-Sca1^{Pos}Axin2^{Pos}. We used males and females C57BL6 and corresponding ob/ob mutant mice to determine the impact of obesity and gender on the functional capacity of the corresponding rMCs-Sca1^{Pos} to trigger AT2 stem cells proliferation.

Our results indicate that an rMC-Sca1^{Pos}Fgf10^{Pos}/LT^{Pos} subpopulation is essential for the proliferation of the AT2 stem cells. This subpopulation is likely different from the previously described MANC. In addition, obesity and gender impact the capacity of rMC-Sca1^{Pos} cells to maintain the proliferation of AT2 stem cells indicating that future therapeutic approaches should be focussed on restoring the function of the mesenchymal niche.

2 | MATERIALS AND METHODS

2.1 | Mice

$Sftpc^{CreERT2/+}$ knock in (gift from Harold Chapman, UCSF), $tdTomato^{flox}$ reporter (Stock 007908, Jacksonlab), $Fgf10^{LacZ}$ reporter (Mailleux

et al., 2005), *Axin2*^{LacZ} reporter (stock 009120, Jackson lab), *Lep*^{ob/ob} (aka *ob/ob*) mutant (stock 000632, Jackson lab) and wild type mice were maintained on the C57BL/6 background. All animal studies were performed according to protocols approved by the Animal Ethics Committee of the Regierungspraesidium Giessen (permit numbers: G7/2017-No. 844-GP and G11/2019-No. 931-GP).

2.2 | Lung dissociation and fluorescence-activated cell sorting

Lungs from C57BL6 (WT) mice were collected at 6-8 weeks of age and processed into a single-cell suspension using collagenase type IV (0.5%ml per lung; Gibco #9001-12-1) and DNase I (SIGMA#DN25). $Cd45^{Neg}Cd31^{Neg}Epcam^{Neg}Sca1^{Pos}$ cells were collected to establish organoid model combined with AT2 cells. The total AT2 population ($Sftpc^{Pos}Tom^{Pos}$ cells) was isolated from lungs of 6-8 weeks old $Sftpc^{CreERT2/+}$; $tdTomato^{flox/flox}$ mice. For the single-cell preparation, lungs were inflated intratracheally with 3 mL dispase (5 U/mL; BD Biosciences #354235) and for further digestion, each lung was incubated in 3 mL dispase solution (5 U/mL) at room temperature for 30 minutes. For the isolation of epithelial cells from the $Sftpc^{Tom}$ lungs, we first sorted a population of $Cd45^{Neg}Cd31^{Neg}Epcam^{Pos}$ cells. To isolate enriched population of mature AT2 cells, we additionally used Lysotracker (100 μM; Green DND-26 fluorescent dye Invitrogen #L7526) and collected $Lyso^{Pos}Tom^{Pos}$ cells. In general, we have considered the fluorescence values higher than 10^3 as a positive selection to gate cells of interest. The values around 0 were gated as a negative selection. In all experiments, we used the negative control to adjust gating to distinguish negative and positive populations.

2.3 | FluoReporter *lacZ* flow cytometry

Fluorescein di (b-D-galactopyranoside) (aka FDG) (Thermo Fischer Scientific #F1930) was used to isolate by FACS, cells expressing ß-galactosidase from $Fgf10^{LacZ}$ and $Axin2^{LacZ}$ reporter lines. Lungs were collected from 6-8 weeks old $Fgf10^{LacZ}$ and $Axin2^{LacZ}$ reporter mice. According to manufacturer's instruction, single-cell suspension and FDG working solution were prewarmed and the cells were resuspended with chloroquine followed by loading by FDG. After incubation for 20 minutes, FDG loading is stopped by adding ice cold staining medium containing propidium iodide and chloroquine. Cells are then placed on ice and incubated with antibodies against Cd45, Cd31, Sca1, and Epcam (for details see Lung dissociation and Fluorescence-Activated Cell Sorting) before sorting using the FACSAria III (BD Bioscience) cell sorter. Cells were sorted through a flow chamber with a 100-μm nozzle tip under 25 psi sheath fluid pressure. Cells were collected in sorting media (advanced DMEM:F12 [Gibco#12634-010] plus 10% FBS and 1% P/S).

2.4 | Alveolar organoid assay

Five thousand $Lyso^{Pos}Tom^{Pos}$ cells (AT2s from adult $Sftpc^{CreERT2/+}$; $tdTomato^{flox/+}$ lungs) and 50 000 rMCs cells were resuspended in 100 μL culture medium (sorting media plus 1% ITS [Gibco # 41400-045]) and mixed 1:1 with 100 μL growth factor-reduced phenol Red-free Matrigel (Corning #356231). Cells were seeded in individual 24-well 0.4 μm Transwell inserts (Falcon, SARSTEDT). After incubation at 37°C for 15 minutes, 500 μL of culture was placed in the lower chamber and the plate was placed at 37°C in 5% CO$_2$/air. The culture medium was changed every other day. ROCK inhibitor (10 μM, Y27632 STEMCELL#72304) was included in the culture medium for the first 2 days of culture. Organoids were counted and measured at day 14. Colony-forming efficiency (CFE) is calculated as the ratio between the numbers of spheres observed over the initial number (5000) of AT2 cells. At day 14, organoids were processed for whole-mount immunofluorescence staining.

2.5 | Whole-mount immunofluorescence staining of organoids

Organoids were fixed in 4% paraformaldehyde for 30 minutes followed by 3× washing steps with PBS and incubation in 0.1% Triton X-100 for 30 min. After washing 3× with PBST, organoids were blocked with 1× TBS, 3% BSA. 0.4% Triton X-100 for 1 hour at room temperature. Organoids were washed and then incubated at 4°C overnight with 1× TBS, 1.5% BSA, 0.2% Triton X-100, and primary antibody against Hopx (1:250 SIGMA #HPA030180). The next day, after 3× washing with TBST for 10 minutes, organoids were incubated with secondary antibodies (AlexaFlour 488 goat anti-Rabbit IgG Green [1:500] Cat. #11034 Invitrogen) at RT and washed three times with TBST before being mounted with Prolong Diamond Anti-fade Mountant with DAPI (Invitrogen 4′,6-diamidino2-phenylindole). Photomicrographs of immunofluorescence staining were taken using a Leica DMRA fluorescence microscope with a Leica DFC360 FX camera (Leica, Wetzlar, Germany). Figures were assembled using Adobe Illustrator.

2.6 | Quantitative RT-PCR

Total RNA was extracted from FACS-sorted $Sca1^{Pos}LT^{hi}$ and $Sca1^{Pos}LT^{Neg}$ cells using RNeasy plus Micro kit (Cat. # 74034 QIAGEN). cDNA was synthesized using QuantiTect Reverse Transcription kit (Cat. #205314 QIAGEN). Quantitative real-time PCR (qRT-PCR) analysis was performed using LightCycler 480 II machine (Roche AppliedScience). Data were presented as expression relative to hypoxanthine-guanine phosphoribosyltransferase (Hprt) for mouse genes.

Primers: *mFgf10*: (For: ATGACTGTTGACATCAGA, Rev: CACT GTTCAGCCTTTTGA), *mPdgfra*: (For: GTCGTTGACCTGCAGTGGA Rev: CCAGCATGGTGATACCTTTG).

2.7 | Co-staining: RNA in situ hybridization assay and IF

Murine lungs were perfused with PBS and fixed in 4% paraformaldehyde according to standard procedures. Next, they were embedded in paraffin and sectioned at 5 μm thickness. RNAscope Mutiplex Fluorescent Reagent Kit v2 assay (document Nr:323100-USM, Advanced Cell Diagnostic, Newark, California) was performed according to the manufacturer's instructions, however, with slight changes in applying standard pretreatment conditions and target retrieval antigen. The pretreatment time was reduced to 7 minutes and the amplification steps were increased to 1 hour. Specific probes were used for the detection of *Fgf10* and *Fgf7* gene expression (*Mm-Fgf10* Cat. #446371, *Mm-Fgf7* Cat. #443521-C3). 3-plex Positive control (Cat. #320881) and 3-plex negative control (Cat. #320871) were carried out using probes specific to murine housekeeping-genes.

These samples were followed by IF for Sftpc. Samples were washed in TBST buffer then incubated at 4°C overnight with 1× TBS, 1.5% BSA, 0.2% Triton X-100, and primary antibody against Sftpc (Anti-Pro-Surfactant Protein C, polyclonal Ab Cat. # AB3786). The next day, after 3× washing with TBST for 10 minutes, samples were incubated with secondary antibodies (AlexaFlour 488 goat anti-Rabbit IgG Green [1:250] Cat. #11034 Invitrogen) at RT and washed three times with TBST before being mounted with Prolong Diamond Anti-fade Mountant with DAPI (Invitrogen 4′,6-diamidino2-phenylindole). Photomicrographs of immunofluorescence staining were taken using a Leica DMRA fluorescence microscope with a Leica DFC360 FX camera (Leica, Wetzlar, Germany). Figures were assembled using Adobe Illustrator.

2.8 | Microarray analysis

Gene expression profiles of two sub-lineages of the resident mesenchymal niche cells were carried out. Purified total RNA was amplified using the Ovation PicoSL WTA System V2 kit (NuGEN Technologies, Bemmel, Netherlands). Per sample, 2 μg amplified cDNA was Cy5-labeled using the SureTag DNA labeling kit (Agilent, Waldbronn, Germany). Hybridization to 8x60K 60mer oligonucleotide spotted microarray slides (Agilent-074809: Catalog gene expression microarray for Mouse, v2 8x60K) and subsequent washing and drying of the slides was performed following the Agilent hybridization protocol in Agilent hybridization chambers, with following modifications: 2 μg of the labeled cDNA were hybridized for 22 hours at 65°C. The cDNA was not fragmented before hybridization. Each sample was processed and hybridized twice (technical replicates).

The dried slides were scanned at 2 μm/pixel resolution using the InnoScan is 900 (Innopsys, Carbonne, France). Image analysis was performed with Mapix 6.5.0 software, and calculated values for all spots were saved as GenePix results files. Stored data were evaluated using the R software and the limma package from BioConductor. Log$_2$ mean spot signals were taken for further analysis. Data was background corrected using the NormExp procedure on the negative control spots and quantile-normalized before averaging. Log$_2$ signals of replicate

spots were averaged, and from several different probes addressing the same gene only the probe with the highest average signal was used. Data from technical replicates was averaged. The data were deposited in a public database (GEO accession: GSE162859). Genes were ranked for differential expression using a moderated *t*-statistic. Pathway analyses were done using gene set tests on the ranks of the *t*-values. Pathways were taken from the KEGG database (http://www.genome.jp/kegg/pathway.html).

Heatmaps are generated from the normalized log$_2$ spot intensities (I) and show the gene-wise z-values (where $z_j = (I_j - \text{mean}(I))/\text{SD}(I)$ for $j = 1,...,n$).

2.9 | Statistics

All results are mean ± SEM. All error bars on graphs represent SEM. Statistical tests are 2-tailed *t* tests. $P \leq .05$ was considered statistically significant.

3 | RESULTS

3.1 | The capacity of Cd45^{Neg}Cd31^{Neg}Epcam^{Neg} resident mesenchymal cells (rMCs) to functionally support the proliferation and differentiation of alveolar epithelial type 2 (AT2) stem cells is associated with Stem cell antigen 1 (Sca1) expression

The aim of this study is to refine the adult lung resident mesenchymal cell population, called thereafter rMC and defined by flow cytometry as Cd45^{Neg}Cd31^{Neg}Epcam^{Neg} cells. It was already shown that the Cd45^{Neg}Cd31^{Neg}Epcam^{Neg}Pdgfrα^{Pos} cell population was capable of sustaining AT2 stem cell renewal using the so-called alveolosphere in vitro assay.[3] In this approach, the use of antibodies against Cd45 and Cd31 allowed removing, from the target subpopulation, the hematopoietic and endothelial cells, respectively.

In the context of a previous milestone study generating organoids in Matrigel arising from a co-culture of Epcam^{High} Cd24^{Low} epithelial cells (previously called epithelial stem/progenitor cells or epiSPC) with rMC-Sca1^{Pos} (Cd45^{Neg}Cd31^{Neg}Epcam^{Neg}Sca1^{Pos}), it was demonstrated that these cells were capable of sustaining the proliferation and differentiation of epiSPCs.[14,15] However, in this study, the impact of the different subpopulations of rMCs on AT2 stem cell proliferation and differentiation was not analyzed.

For this purpose, we have sorted an enriched population of mature AT2 cells from the *Sftpc*$^{CreERT2/+}$; *Tomato*$^{flox/+}$ lungs. We started first by isolating Cd31^{Neg}Cd45^{Neg}Epcam^{Pos} cells and then applied two successive and stringent sorting approaches: first using LysoTracker, a fluorescent dye that labels acidic compartments found abundantly in the lamellar bodies of AT2 cells and second, using the tomato reporter expressed specifically in AT2 cells (Figure 1A). In addition, we sorted also rMCs-Sca1^{Pos} (Cd45^{Neg}Cd31^{Neg}Epcam^{Neg}Sca1^{Pos}) as well as rMCs-Sca1^{Neg} (Cd45^{Neg}Cd31^{Neg}Epcam^{Neg}Sca1^{Neg}). In order to have

sufficient cells to carry out our assay, we pooled the lungs of four adult (6-8 weeks old) C57BL/6 mice. This allowed us to carry out 6 independent cocultures. Sca1^{Pos} cells represent around 25% of the total rMC population (Figure 1A). When co-cultured with sorted mature AT2s, rMC-Sca1^{Pos} led to the formation of organoids (Figure 1B) with a colony forming efficiency of 5% (Figure 1C) which is in line with previously published alveolosphere experiments. Interestingly, rMCs-Sca1^{Neg} fail to sustain alveolosphere formation (Figure 1B). The difference in organoid size and CFE is highly significant between the two rMC subpopulations (Figure 1C, $P < .01$).

3.2 | rMCs-Sca1^{Pos} can be further functionally subdivided for the proliferation and differentiation of AT2 stem cells on the basis of LipidTOX staining

To better characterize rMCs-Sca1^{Pos} lung cells and in particular whether this population may include the lipofibroblasts (LIFs), we used LipidTOX (LT), an efficient fluorescent stain for neutral lipid. As LIFs are abundant in neutral lipid droplets, LT has been previously used to quantify LIF population during lung development.[2]

Sorted rMCs-Sca1^{Pos}LT^{High} and rMCs-Sca1^{Pos}LT^{Neg} were tested functionally in the alveolosphere model for their capacity to induce the proliferation and differentiation of AT2 stem cells (Figure 2A). For this experiment, we pooled the cells from three mice and carried four independent co-cultures. When co-cultured with sorted mature AT2s, rMCs-

Sca1^{Pos}LT^{High} led to the formation of organoids (Figure 2B) with a colony forming efficiency of 2% (Figure 2C) while rMCs-Sca1^{Pos}LT^{Neg} failed to sustain organoid formation. We also carried out at day 14, Immunofluorescence (IF) for LT (LIF marker), Hopx (AT1 cell marker), and DAPI in conjunction with the detection of the endogenous tomato reporter (Figure 2B). Our results indicate that LT^{Pos} cells are located in the periphery of each organoid. In addition, we observed abundant expression of Hopx within the organoid indicating proper AT2 to AT1 differentiation. RT-qPCR was also carried out to quantify the expression of *Fgf10* and *Pdgfra*, two well-known markers enriched in LIFs (Figure 2D). Our results indicate a trend toward an increase in the expression of *Fgf10* and *Pdgfra* in rMCs-Sca1^{Pos}LT^{High} compared to rMCs-Sca1^{Pos}LT^{Neg} ($n = 3$ independent mice) (Figure 2D). These results are in line with the previous observation that *Fgf10* and *Pdgfra* are also expressed in cells other than LIFs.[2,16] Overall, our data therefore support the previous conclusion that it is the LIF subpopulation of the rMCs that can preferentially support AT2 stem cell survival and differentiation.

3.3 | Fgf10^{Pos} cells represent a niche for AT2 cells

We have previously reported that during development, a subset of Fgf10^{Pos} cells are progenitors for lipofibroblasts (LIFs) in the late stage of development and postnatally. We have also reported that during the early postnatal stage of lung development, only 28% of the LIFs express *Fgf10* indicating that the LIFs, like Fgf10^{Pos} cells[5], are a
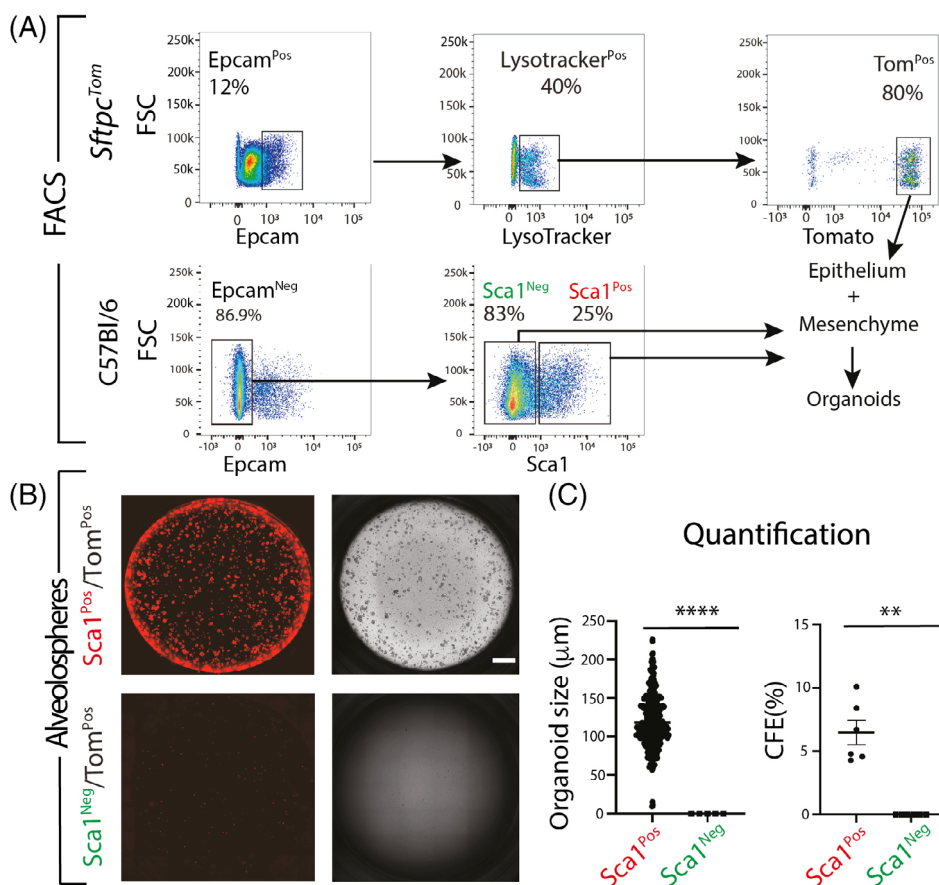

FIGURE 1 Sca1 expression in combination with the alveolosphere assay separates functionally the lung resident mesenchymal cells. A, Gating strategy to sort mature AT2 (Epcam^{Pos}Lysotracker^{Pos}Tom^{Pos}) from *Sftpc^{Tom}* as well as rMc-Sca1^{Pos} (Cd31^{Neg}Cd45^{Neg}Epcam^{Neg}Sca1^{Pos}) and rMC-Sca1^{Neg} (Cd31^{Neg}Cd45^{Neg}Epcam^{Neg}Sca1^{Neg}) cells from C57BL6 (WT) mice. B, Alveolosphere assay at day 14: Co-culture of mature AT2 with rMC-Sca1^{Pos} or rMC-Sca1^{Neg} cells. C, Quantification of the organoids; organoid size, and colony forming efficiency of six independent experiments ($n = 6$). Scale bar = 50 μm

FIGURE 2 LipidTOX staining identifies a subpopulation of rMC-Sca1^{Pos} cells supporting the proliferation and differentiation of AT2 stem cells. A, *Sftpc*^{Tom} and C57BL6 (WT) mice in 6-8 weeks of age were used to sort Lyso^{Pos}Tom^{Pos} mature AT2 cells and rMC-Sca-1^{Pos}LT^{High} or rMC-Sca-1^{Pos}LT^{Neg} resident stromal cells. Mixture of cells were seeded in Matrigel in 24-well Transwell. B, Fluorescence and bright field picture of representative wells at day 14. IF staining of organoids for DAPI, RFP (surrogate for Sftpc, an AT2 cell marker), and Hopx (AT1 cell marker) indicating that lipofibroblasts (rMC-Sca-1^{Pos}LT^{High}) support AT2 stem cell differentiation into AT1 cells (Scale bar = 100 μm). C, Quantification of colony forming efficiency (2.3 vs 0 in rMC-Sca-1^{Pos}LT^{High} vs rMC-Sca-1^{Pos}LT^{Neg}, respectively (*P* value 0.001). D, *Fgf10* and *Pdgfra* gene expression were assessed by qRT-PCR in rMC-Sca-1^{Pos}LT^{High} vs rMC-Sca-1^{Pos}LT^{Neg}. Quantification of gene expression were normalized to *Hprt*. Scale bar = 50 μm
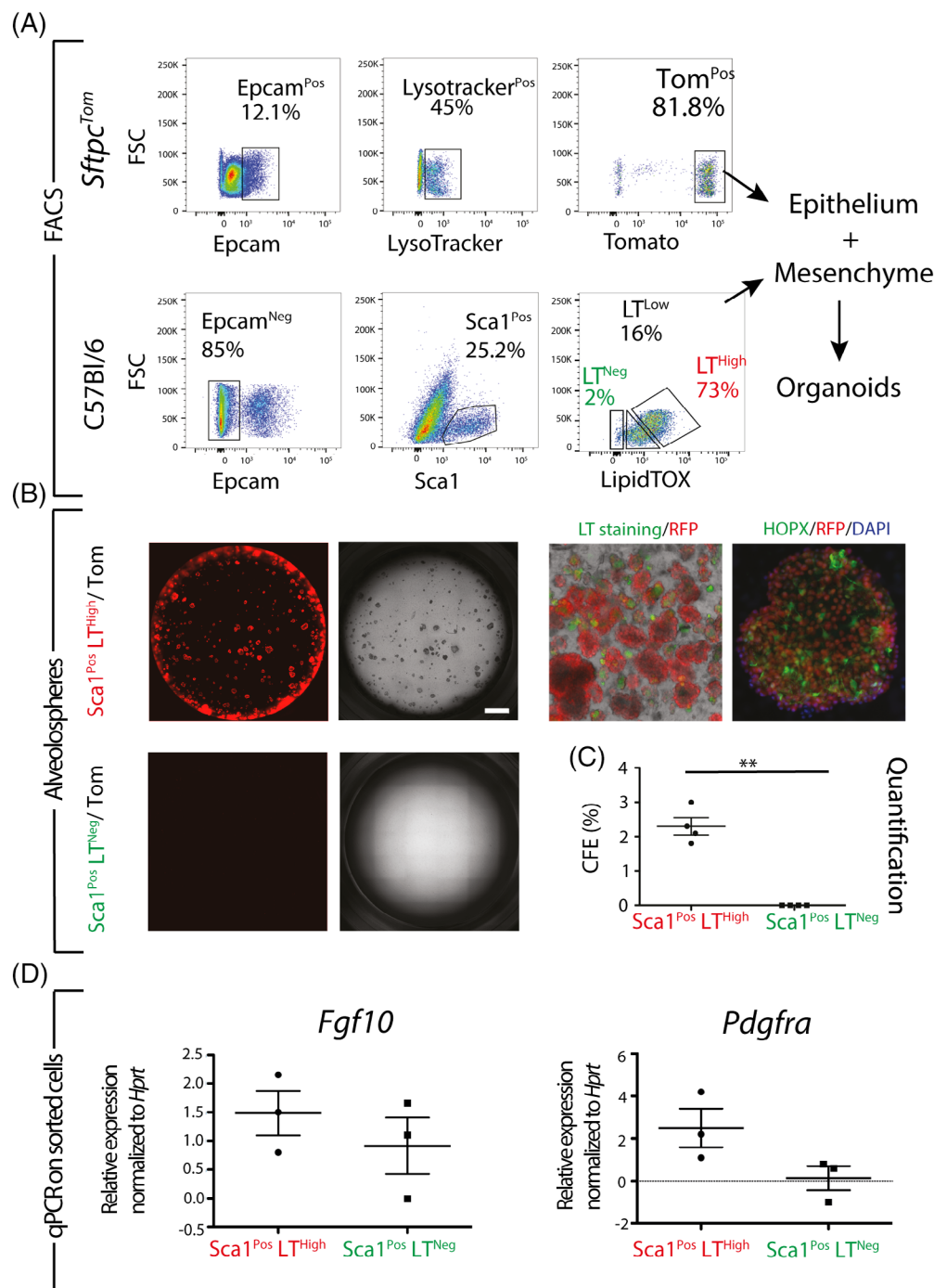
heterogenous population. To functionally evaluate the difference between rMCs-Sca1^{Pos}Fgf10^{Pos} and rMCs-Sca1^{Pos}Fgf10^{Neg} cells, we used the *Fgf10*^{LacZ} reporter line in combination with the ß-galactosidase fluorescent substrate FDG to sort, from rMCs, enriched populations of FDG^{Pos} (Fgf10^{Pos}) and FDG^{Neg} (Fgf10^{Neg}) cells. We then isolated the Sca1^{Pos} fraction for each subpopulation. Our results indicate that rMCs-Sca1^{Pos}Fgf10^{Pos} represents around 33% of the rMCs-Fgf10^{Pos} and 25% of the rMCs-Sca1^{Pos}. These results indicate that the rMCs-Sca1^{Pos} as well as the rMCs-Fgf10^{Pos} subpopulation are indeed heterogeneous (Figure 3A). As previously described, we have co-cultured rMCs-Sca1^{Pos}Fgf10^{Pos} as well as rMCs-Sca1^{Pos}Fgf10^{Neg} cells with AT2 in our alveolosphere assay. Our

results indicate that organoid only form with rMCs-Sca1^{Pos}Fgf10^{Pos} with a CFE of 4% (n = 4 independent experiments) (Figure 3B,D). rMCs-Sca1^{Pos}Fgf10^{Neg} are not capable of eliciting organoid formation. IF staining of the organoids for Hopx show that the AT2 cells properly differentiate into AT1 cells (Figure 3C).

3.4 | Comparison of rMCs-Sca1^{Pos}Fgf10^{Pos} vs rMCs-Sca1^{Pos}Axin2^{Pos}

Fgf10^{Pos} cells are progenitor for lipofibroblast. LIF in alveolar region are functionally important to support AT2 cells during lung
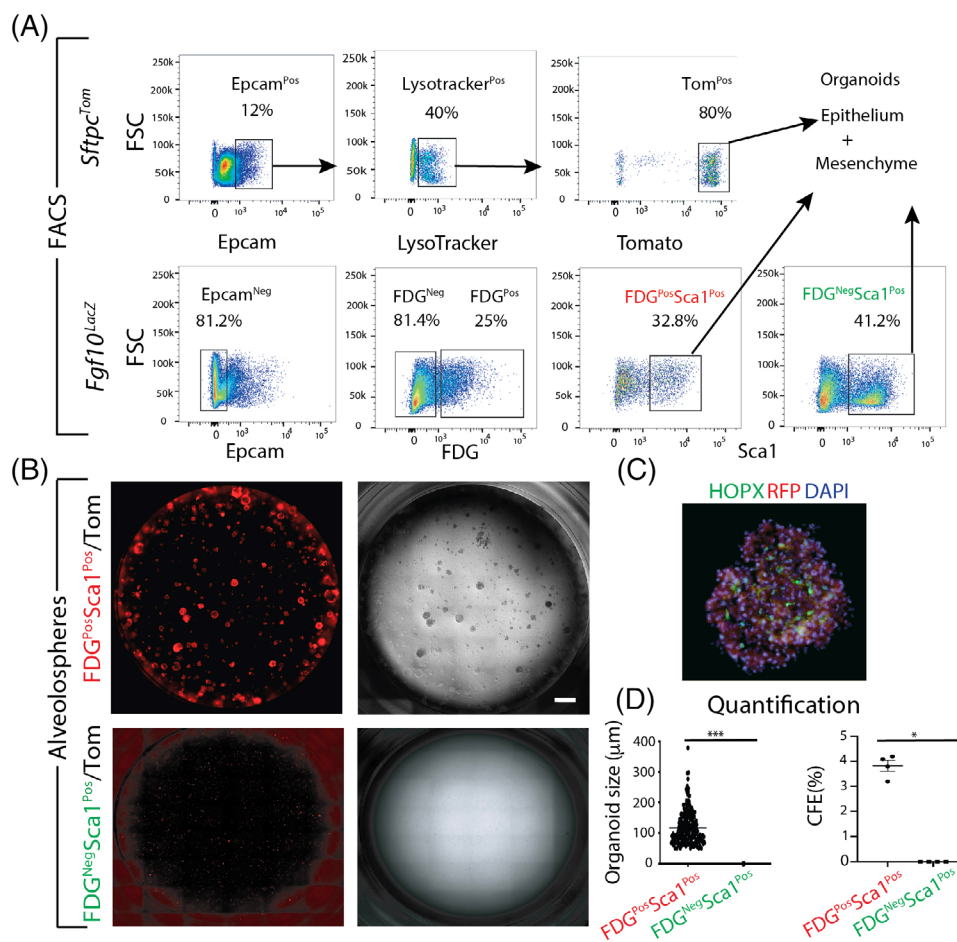
FIGURE 3 rMC-Sca1^{Pos}Fgf10^{Pos} cells are supporting the proliferation and differentiation of AT2 stem cells. A, Gating strategy to sort mature AT2 cells from *Sftpc^{Tom}* lungs as well as rMC-Sca1^{Pos}Fgf10^{Pos} and rMC-Sca1^{Pos}Fgf10^{Neg} cells from *Fgf10^{LacZ}* lungs using the FDG fluorescent substrate for ß-galactosidase. B, Alveolosphere assay showing that only co-culture with rMC-Sca1^{Pos}Fgf10^{Pos} leads to organoid formation. C, IF staining against for Hopx and DAPI. D, Quantification of organoid size and CFE with rMC-Sca1^{Pos}Fgf10^{Pos} or rMC-Sca1^{Pos}Fgf10^{Neg} (n = 4). Scale bar =100 µm

development and postnatal stages. In addition, Axin2, a marker for Wnt signaling activation, is expressed in a subset of mesenchymal cells in the adult lung.[17,18] It has been reported that 74% of Axin2^{Pos} cells in the alveolar region are also expressing Pdgfrα. Axin2^{Pos} Pdgfrα^{Pos} mesenchymal cells are called mesenchymal alveolar niche cells (MANC) and are located closed to AT2 cells. Using the alveolosphere model, they have been reported to sustain AT2 stem cell proliferation and differentiation. As these cells have been described to express *Fgf7* and not *Fgf10*,[6] we propose that rMCs-Sca1^{Pos}Fgf10^{Pos} and rMCs-Sca1^{Pos}Axin2^{Pos} represent two independent pools of niche cells for AT2 stem cells.

To better characterize these two rMC subpopulations, we used specific reporter lines; *Fgf10^{LacZ}* and *Axin2^{LacZ}* to monitor the distribution of LipidTOX staining in these two sub-lineages. By using FACSAria III cell sorter, we analyzed 100 000 events, each sample contained harvested lung from one mouse -with the same age range (6-8 weeks old). Cd45^{Neg}Cd31^{Neg}Epcam^{Neg}Sca1^{Pos} sorted cells were processed for further analysis (Figure 4A). For *Fgf10^{LacZ}* lungs, we found 25% FDG^{Pos} (rMC-Sca1^{Pos}Fgf10^{Pos}) cells out of total rMC-Sca1^{Pos}. For *Axin2^{LacZ}* lungs, our results indicate around 10% FDG^{Pos} (rMC-Sca1^{Pos}Axin2^{Pos}) cells out of total rMC-Sca1^{Pos}. Further analysis based on LipidTox staining indicate that 85% of Fgf10^{Pos} and 98% of rMC-Sca1^{Pos}Axin2^{Pos} cells were also LT^{High} cells (Figure 4B,C, respectively). Based on LT staining, we

also report that most of the rMCs-Sca1^{Pos}Fgf10^{Neg} as well as rMCs-Sca1^{Pos}Axin2^{Neg} subpopulations contain a high percentile of LT$^{Low/High}$ cells suggesting again a functional heterogeneity at the level of the LIFs (in regards to the maintenance of AT2 stem cell proliferation) based on whether they express or not *Fgf10* or *Axin2*.

In order to better define at the transcriptomic level, the difference between rMCs-Sca1^{Pos}Fgf10^{Pos} and rMCs-Sca1^{Pos}Axin2^{Pos}, we performed gene array analysis using the Agilent platform. Figure 4D shows top 100 genes which differentially expressed between rMCs-Sca1^{Pos}Fgf10^{Pos} and rMCs-Sca1^{Pos}Fgf10^{Neg} subsets (see Figure S1 for higher magnification of the heatmap). The genes differentially regulated between these two subsets were then evaluated in rMCs-Sca1^{Pos}Axin2^{Pos} cells. Our results indicate that several markers such as *Ackr4, Jchain, Cd46, Alox5, Nfam1* and *Col10a1* are differentially expressed between rMCs-Sca1^{Pos}Fgf10^{Pos} and rMCs-Sca1^{Pos}Axin2^{Pos} and therefore could be used in the future to label these mesenchymal subpopulations. KEGG analysis of rMCs-Sca1^{Pos}Axin2^{Pos} vs rMCs-Sca1^{Pos}Fgf10^{Pos} indicates an upregulation of metabolic pathways, RNA transport, DNA replication as well as cell cycle indicating that the Axin2^{Pos} cells are metabolically active and proliferative (Table S1). Altogether, our data notably suggest that rMCs-Sca1^{Pos}Fgf10^{Pos} cells are likely different from rMCs-Sca1^{Pos}Axin2^{Pos} cells.
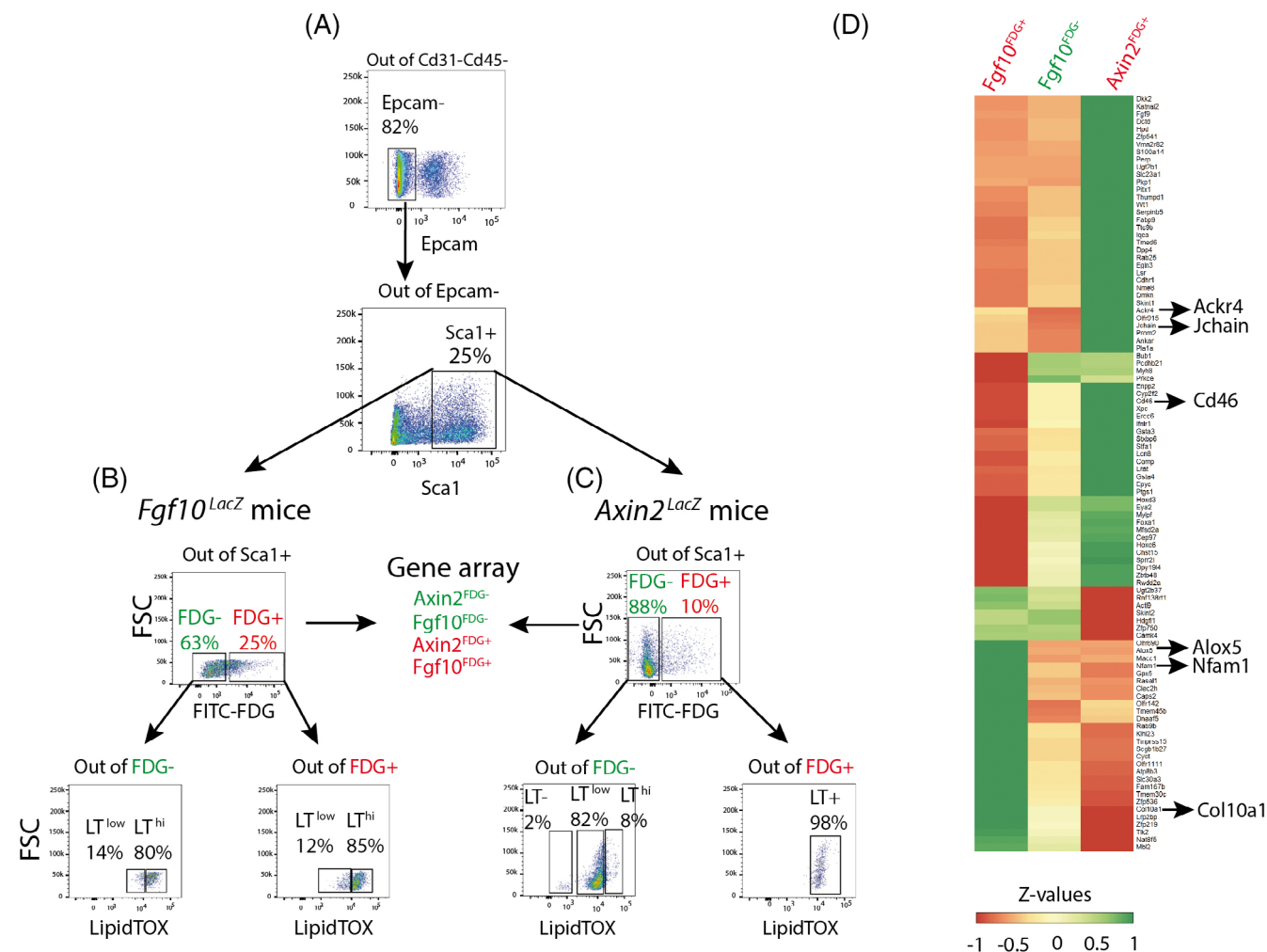
FIGURE 4 Comparison of rMC-Sca1^Pos Fgf10^Pos vs rMC-Sca1^Pos Axin2^Pos. A, Single cell suspension from the adult lungs of *Fgf10^LacZ* and *Axin2^LacZ* reporter lines were processed by flow for Cd31, Cd45, Epcam and Sca1 expression to isolate rMC-Sca1^Pos. B,C, Staining with the FDG fluorescent substrate for ß-galactosidase allowed to separate further the rMC-Sca1^Pos into rMC-Sca1^Pos Fgf10^Pos and rMC-Sca1^Pos Fgf10^Neg (B) as well as rMC-Sca1^Pos Axin2^Pos and rMC-Sca1^Pos Axin2^Neg (C). Further staining with LipidTOX allowed to quantify the abundance of LT^High in each subpopulation. D, Heatmap is representing top 100 genes which are differentially expressed between rMC-Sca1^Pos Fgf10^Pos and rMC-Sca1^Pos Fgf10^Neg. Note that the genes which are downregulated in rMC-Sca1^Pos Fgf10^Pos are upregulated in rMC-Sca1^Pos Axin2^Pos and vice versa. The arrows show some of the selected genes among the 100 genes

3.5 | *Fgf10* expressing cells are located close to Sftpc^Pos cells

To investigate the relative interaction between *Fgf10* expressing cells and AT2 cells, we combined the in situ hybridization technique for detecting *Fgf10* mRNA expression with immunofluorescence staining for pro-SPC in adult wild type lungs. We found that 28% ± 0.5% (n = 3) of total *Fgf10* expressing cells are located close to pro-SPC expressing cells (Figure 5A). This number is very similar to the one we reported before in the newborn lung using the *Fgf10^LacZ* reporter.[2] This observation suggests that a subset only of the *Fgf10* expressing cells constitutes a critical component of the alveolar niche that may robustly communicate with AT2 cells. To better define the heterogeneity of AT2 stromal niche, we have also performed co-staining of *Fgf7* mRNA and Sftpc. *Fgf7* expression has been proposed

to be a hallmark of the MANC population. To validate the *Fgf7* mRNA probe, we used *Fgf7* KO adult lungs. While a clear signal was obtained with a positive control probe provided by the manufacturer, the *Fgf7* mRNA probe failed to generate a signal in the *Fgf7* KO lungs (Figure S2) indicating that the signal observed in wild type lung is specific (Figure 5B). We found that around only 2.0% ± 0.2% (n = 3) of *Fgf7* expressing cells are in vicinity of Sftpc^Pos cells (Figure 5B). Finally, we performed a co-staining for *Fgf7* and *Fgf10* mRNA using different fluorescent labeled probes. Our results indicate that 15.7% ± 1.3% (n = 3) of total cells are *Fgf7* expressing cells vs 25.4% ± 0.9% (n = 3) for *Fgf10* expressing cells. Finally, 4.0% ± 0.3% (n = 3) of total cells are double positive *Fgf10/Fgf7* cells (Figure 5C). Taken together, these data suggest that the rMCs-Sca1^Pos Fgf10^Pos are distinct from Fgf7^Pos MANC, while both subpopulations are located close to AT2 cells.
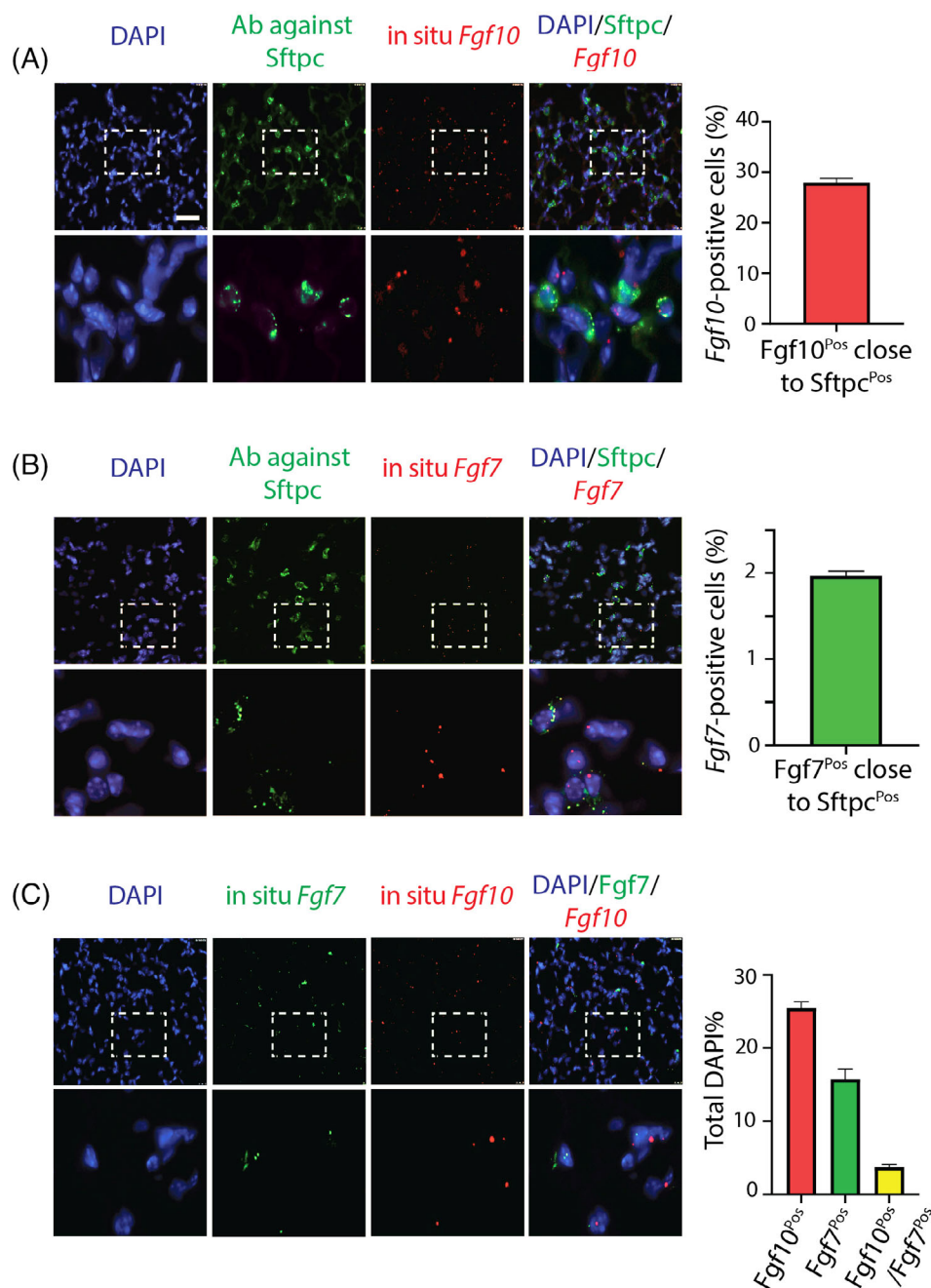
(A)

(B)

(C)

FIGURE 5 Analysis and comparison of *Fgf10* and *Fgf7* mRNA expression in relation to pro-Sftpc[Pos] cells in the adult mouse lung. A, In situ hybridization for *Fgf10* mRNA (in red) and IF staining against for pro-Sftpc (in green). Low and high magnification. Quantification of *Fgf10* expressing cells close to Pro-Sftpc[Pos] cells. B, In situ hybridization for *Fgf7* mRNA (in red) and IF staining against for pro-Sftpc (in green). Low and high magnification. Quantification of *Fgf7* expressing cells close to Pro-Sftpc[Pos] cells. C, Co-staining of *Fgf10* and *Fgf7* expressing cells. Quantification of *Fgf7*, *Fgf10* as well as *Fgf7/Fgf10* expressing cells compared to total cells. Scale bar for low magnification: 50 μm and Scale bar for high magnification 200 μm

3.6 | rMCs-Sca1[Pos] are impacted by obesity and gender

Massive damages to the AT2s occur following various injuries such as viral infection. As a consequence, the transdifferentiation of the LIFs into activated MYFs has been proposed, thereby leading to fibrosis formation.[7] Obesity/diabetes and gender are thought to be aggravating pre-existing conditions predicting the severity of the disease.[12]

To explore the impact of obesity/diabetes and gender on the functionality of the rMCs-Sca1[Pos] cells, we used 6-8 weeks C57BL6 males and females as well as *Leptin*-deficient *ob/ob* (aka *ob/ob*) mutant male and female mice (n = 3 for each gender and for WT and mutant). Figure 6A shows the analysis by flow cytometry of rMCs-Sca1[Pos] in C57BL/6 mice vs C57BL/6 Leptin-deficient *ob/ob* mice. Interestingly, a drastic reduction

of the percentile of rMCs-Sca1[Pos] is observed in *ob/ob* mice compared to wild type mice (27.7% vs 9%, respectively). We also functionally tested the rMCs-Sca1[Pos] from these different mice by co-culturing them with sorted AT2 cells using the alveolosphere assay. When the rMCs-Sca1[Pos] are isolated from *ob/ob* male mice presenting the two risk factors, obesity and male (Figure 6B), we observed a complete absence of organoid formation (n = 3). However, when rMCs-Sca1[Pos] are isolated from female *ob/ob* mice presenting only obesity as a risk factor, a significant number of organoids are present (3% CFE, n = 3). This CFE is, however, lower than the one observed in non-obese C57BL6 female wild type mice (5% CFE, n = 3) indicating that obesity alone is already impacting the functionality of the rMCs-Sca1[Pos]. Interestingly, non-obese C57BL6 male wild type mice display also a reduced CFE compared to non-obese C57BL6 female wild type mice (2% vs 5%, respectively, n = 3) indicating that the
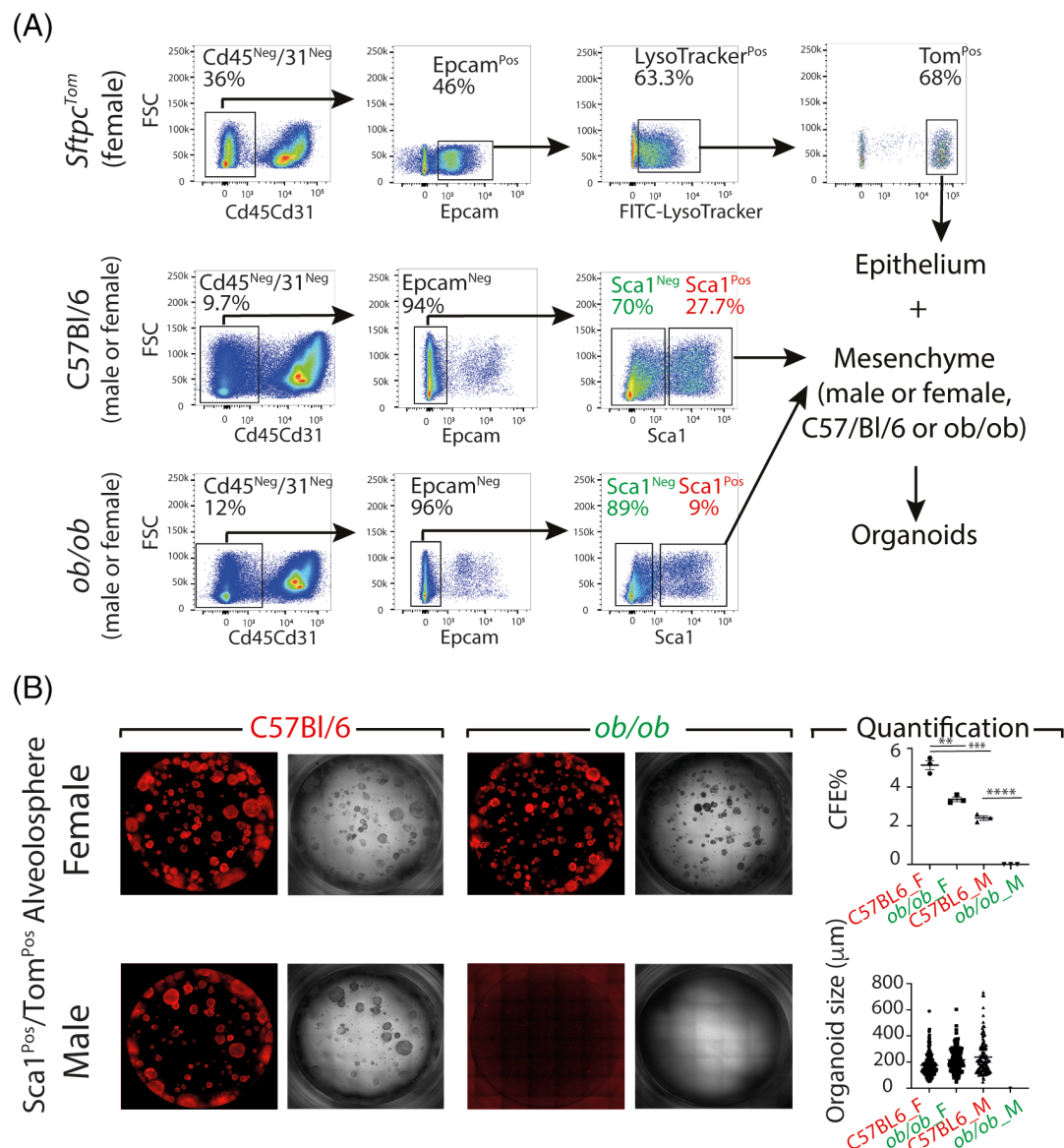
FIGURE 6 rMC-Sca1^{Pos} cells are affected by obesity and gender. A, Flow cytometry analysis and gating strategy to sort mature AT2 cells from *Sftpc^{Tom}* as well as rMC-Sca1^{Pos} from male and female C57BL/6 mice, and male and female *ob/ob* mice (n = 3 for each genotype and gender). B, Alveolosphere culture after 14 days and corresponding quantification of organoid size and colony forming efficiency (n = 3 animals per condition). Scale bar = 50 μm

gender alone is also impacting the functionality of the rMCs-Sca1^{Pos}. We also observed that age was also having the same effect than obesity and gender on the capacity of the rMCs-Sca1^{Pos} to maintain the proliferation of the AT2 stem cells (data not shown).

4 | DISCUSSION

4.1 | rMC-Sca1^{Pos}Fgf10^{Pos} are different from the rMC-Sca1^{Pos}Axin2^{Pos}

A major problem arising from key publications using flow cytometry as a primary experimental approach is the lack of independent studies reporting the reproducibility of the results. This is due in part to the type of flow sorter used, the sophisticated flow cytometry protocols,

including the gating conditions used and the lack of comparison with other endogenous population at the time of the sort as internal controls. This is particularly crucial in the context of the lung mesenchyme which is still a huge black box both in human and in mice in spite of recent scRNA seq studies.[19] In our study, we adopted an unbiased and reproducible FACS strategy to sort both epithelial and mesenchymal populations. We used Sca1 as a resident mesenchymal cell marker to refine the rMC population. In previous studies, Cd45^{Neg}Cd31^{Neg}Sca1^{Pos} cells were detectable by flow cytometry in the postnatal lung coincidently with the transition from the saccular to the alveolar stage of lung development. This population also co-expressed Cd34, Thy1 (Cd90), as well as Pdgfrα and was proposed to mark LIFs.[20] Interestingly, our gene array data shows that Cd90 is highly expressed in rMC-Sca1^{Pos}Fgf10^{Pos} compared to rMC-Sca1^{Pos}Axin2^{Pos} (data not shown). In another study, it was shown

that Cd45[Neg]Cd31[Neg]Epcam[Neg]Sca1[Pos] (rMC-Sca1[Pos] cells) could be refined into two main subpopulations, namely Cd166[Pos]Cd90[Neg] and Cd166[Neg]Cd90[Pos]. The Cd166[Neg]Cd90[Pos] subpopulation contained undifferentiated mesenchymal progenitors capable of differentiating toward the LIF and the MYF lineage while the Cd166[Pos]Cd90[Neg] subpopulation contained more differentiated mesenchymal cells already committed to the MYF lineage. Additionally, the Cd166[Neg]Cd90[Pos] expressed high levels of *Fgf10*.[15] Further organoid-based experiments indicated that Cd166[Neg] compared Cd166[Pos] displayed higher activity in supporting the proliferation of epiSPC. In vitro culture of rMC-Sca1[Pos] cell showed that these cells lost their capacity to maintain epiSPC proliferation over time. This activity could be completely rescued by co-culturing these rMC-Sca1[Pos] cells with the TGFb1-inhibitor SB431542. Such treatment was associated with the upregulation of endogenous *Fgf10* expression in in vitro cultured rMC-Sca1[Pos].[14] Finally, a drastic increase in CFE was observed upon treatment of rMC-Sca1[Pos]-epiSPC co-culture with recombinant FGF10. In these experimental conditions, FGF7 did not display such activity.[15] Taken together, our results indicate that rMC-Sca1[Pos]Fgf10[Pos] correspond to a specifically enriched population of LIFs capable of maintaining AT2 stem cell proliferation and differentiation. A recent milestone study published in Cell described a mesenchymal cell subpopulation called MANC (Mesenchymal Alveolar Niche Cells), which was positive for *Axin2*, *Pdgfra*, *Wnt2*, *Il6*, and *Fgf7*.[6] MANCs are located close to AT2s and sustain in vitro the proliferation and differentiation of AT2 stem cells. The current knowledge, before this study was therefore that the MANC were considered at the top of a hierarchy of mesenchymal niche cells and were likely to be important for both homeostasis and repair after injury. The current study brings into light a novel challenger for this important role. Our results indicate that rMC-Sca1[Pos]Fgf10[Pos] are likely different from the rMC-Sca1[Pos]Axin2[Pos] (aka the MANC, but isolated in our experimental conditions) but has, nonetheless a similar function in regards to the AT2 stem cells. In addition, we cannot exclude the possibility that AT2 stem/progenitor cells are also heterogeneous, and that rMC-Fgf10[Pos] and rMC-Axin2[Pos] (MANC) may be targeting different AT2 stem/progenitor cell subsets.[17,18]

4.2 | Are the rMC-Sca1[Pos]Fgf10[Pos] more relevant than the rMC-Sca1[Pos]Axin2[Pos] for the repair process after injury?

Given the fact that both subpopulations appear to sustain the proliferation and differentiation of AT2 stem cells in vitro, a natural question is therefore whether they have redundant functions or whether one population appears to be more crucial than the other. From the angle of Fgf signaling and based on the consequence of *Fgf7* vs *Fgf10* gene inactivation in mice, we can conclude that rMC-Sca1[Pos]Fgf10[Pos] are likely important. *Fgf10* inactivation leads to lung agenesis[21] while *Fgf7* null mice are viable and display no obvious lung phenotype.[22] Changes in endogenous *Fgf10* expression has been correlated with disease progression and/or repair after lung injury both in mice and humans.[23-25] Evidence for such a role for Fgf7 in the embryonic or

adult lung in human or mice are still lacking in spite of the fact that Fgf7 was discovered 7 years before Fgf10.[26,27] Another important question is whether it matters if mesenchymal niche cells express Fgf7 vs Fgf10 as they are both ligands acting through Fgfr2b. Indeed, it does matter as Fgf7 and Fgf10, although belonging to the same Fgf subfamily of paracrine growth factors elicit different biological activities on isolated lung epithelium grown in Matrigel in vitro.[4] During the process of lung branching, Fgf10 induces the formation of new buds by a process of chemotaxis, while Fgf7 triggers the proliferation of the epithelium leading to the formation of a cyst-like structure. Mass spectrometry studies demonstrated that Fgf10 differentially stimulated the phosphorylation of tyrosine 734 of Fgfr2b and the recruitment of the SH3-domain-binding protein 4 (SH3bp4).[28] Tyrosine 734 phosphorylation controls the trafficking route of the receptor after internalization, allowing receptor recycling at the cell surface and sustained Akt and Shc phosphorylation. Knockdown of SH3bp4 or ectopic expression of a Y734F-mutated form of Fgfr2b in lung explants cultured in vitro modified the biological activity triggered by Fgf10 from chemotactic (bud formation) to proliferative (cyst-like structure).

4.3 | The activity of the rMc-Sca1[Pos] cells is impacted by obesity and gender

In the context of lung fibrosis, the accumulation of activated MYF-producing extracellular matrix components modifies the lung structure and negatively impacts gas exchange. The LIF to MYF reversible differentiation switch appears to be a key process in fibrosis formation and resolution. Moreover, this transition was also shown in vitro in response to hyperoxia, as a key event in bronchopulmonary dysplasia (BPD). AT2 cells express angiotensin-converting enzyme II (ACEII), a main receptor for SARS-CoV-2.[30] Interestingly, SARS-CoV-2 induces the expression of transforming growth factor β (TGF-β),[31] which has been described to trigger the LIF to activated MYF transition. Such transition can be reversed by the administration of a PPARγ agonist (Rosiglitazone) as well as by the antidiabetic drug metformin.[7,8] Interestingly, metabolic dysregulation such as the one observed in obese patients has been associated with a worst prognostic in case of COVID-19. A similar conclusion has been reached for the gender as well as for the age. Indeed, we can detect the impact of obesity and gender on the functionality of the rMC-Sca1[Pos] cells to sustain AT2 stem cell proliferation and differentiation. Our findings open the way to screen for drugs capable of restoring the stromal niche capabilities.

5 | CONCLUSION

In this study, we have shown that rMC-Sca1[Pos]Fgf10[Pos]/LT[Pos] is an important rMC subset allowing the proliferation of AT2 stem cells. We propose that this activity can be negatively impacted by many factors such as obesity and gender. In the future, restoring rMC function may be instrumental to optimize repair after injury.

CONFLICT OF INTEREST

The authors declared no potential conflicts of interest.

AUTHOR CONTRIBUTIONS

S.T.: performed all experiments, conceived the project and wrote the manuscript, contributed to the article and approved the submitted version; M.H and A.I.V.A.: performed FACS analysis and sorting for samples, contributed to the article and approved the submitted version; J.W.: carried out the bioinformatics analysis, contributed to the article and approved the submitted version; S.H. and C.C.: contributed to the article and approved the submitted version; J.Z. and S.B.: conceived the project and wrote the manuscript, contributed to the article and approved the submitted version.

DATA AVAILABILITY STATEMENT

The data that support the findings of this study are openly available in GEO accession reference number GSE162859.

ORCID

Saverio Bellusci [iD] https://orcid.org/0000-0001-5987-4579

REFERENCES

1. Phan SH. Genesis of the myofibroblast in lung injury and fibrosis. *Proc Am Thorac Soc*. 2012;9:148-152.
2. Al Alam D, El Agha E, Sakurai R, et al. Evidence for the involvement of fibroblast growth factor 10 in lipofibroblast formation during embryonic lung development. *Development*. 2015;142: 4139-4150.
3. Barkauskas CE, Cronce MJ, Rackley CR, et al. Type 2 alveolar cells are stem cells in adult lung. *J Clin Invest*. 2013;123:3025-3036.
4. Bellusci S, Grindley J, Emoto H, Itoh N, Hogan BL. Fibroblast growth factor 10 (FGF10) and branching morphogenesis in the embryonic mouse lung. *Development*. 1997;124:4867-4878.
5. El Agha E, Herold S, Al Alam D, et al. Fgf10-positive cells represent a progenitor cell population during lung development and postnatally. *Development*. 2014;141:296-306.
6. Zepp JA, Zacharias WJ, Frank DB, et al. Distinct mesenchymal lineages and niches promote epithelial self-renewal and myofibrogenesis in the lung. *Cell*. 2017;170:1134-1148.e10.
7. El Agha E, Moiseenko A, Kheirollahi V, et al. Two-way conversion between lipogenic and myogenic fibroblastic phenotypes marks the progression and resolution of lung fibrosis. *Cell Stem Cell*. 2017;20: 261-273.e3.
8. Kheirollahi V, Wasnick RM, Biasin V, et al. Metformin induces lipogenic differentiation in myofibroblasts to reverse lung fibrosis. *Nat Commun*. 2019;10:2987.
9. Günther A, Korfei M, Mahavadi P, et al. Unravelling the progressive pathophysiology of idiopathic pulmonary fibrosis. *Eur Respir Rev*. 2012;21:152-160.
10. Vasarmidi E, Tsitoura E, Spandidos D, et al. Pulmonary fibrosis in the aftermath of the Covid-19 era (Review). *Exp Ther Med*. 2020;20: 2557-2560.
11. Rogliani P, Calzetta L, Coppola A, et al. Are there pulmonary sequelae in patients recovering from COVID-19? *Respir Res*. 2020;21:4-7.
12. Ritter A, Kreis NN, Louwen F, et al. Obesity and covid-19: molecular mechanisms linking both pandemics. *Int J Mol Sci*. 2020;21: 1-27.
13. Louwen F, Ritter A, Kreis NN, Yuan J. Insight into the development of obesity: functional alterations of adipose-derived mesenchymal stem cells. *Obes Rev*. 2018;19:888-904.
14. McQualter JL, McCarty RC, Van der Velden J, et al. TGF-β signaling in stromal cells acts upstream of FGF-10 to regulate epithelial stem cell growth in the adult lung. *Stem Cell Res*. 2013;11:1222-1233.
15. McQualter JL, Yuen K, Williams B, et al. Evidence of an epithelial stem/progenitor cell hierarchy in the adult mouse lung. *Proc Natl Acad Sci USA*. 2010;107:1414-1419.
16. Ntokou A, Klein F, Dontireddy D, et al. Characterization of the platelet-derived growth factor receptor-α-positive cell lineage during murine late lung development. *Am J Physiol Lung Cell Mol Physiol*. 2015;309:L942-L958.
17. Zacharias WJ, Frank DB, Zepp JA, et al. Regeneration of the lung alveolus by an evolutionarily conserved epithelial progenitor. *Nature*. 2018;555:251-255.
18. Nabhan AN, Brownfield DG, Harbury PB, Krasnow MA, Desai TJ. Single-cell Wnt signaling niches maintain stemness of alveolar type 2 cells. *Science*. 2018;359:1118-1123.
19. Travaglini KJ, Nabhan AN, Penland L, et al. A molecular cell atlas of the human lung from single-cell RNA sequencing. *Nature*. 2020;587: 619-625.
20. McQualter JL, Brouard N, Williams B, et al. Endogenous fibroblastic progenitor cells in the adult mouse lung are highly enriched in the Sca-1 positive cell fraction. *STEM CELLS*. 2009;27:623-633.
21. Sekine K, Ohuchi H, Fujiwara M, et al. Fgf10 is essential for limb and lung formation. *Nat Genet*. 1999;21:138-141.
22. Finch PW, Rubin JS, Miki T, et al. Human KGF is FGF-related with properties of a paracrine effector of epithelial cell growth. *Science (80–)*. 1989;245:752-755.
23. Volckaert T, Yuan T, Chao CM, et al. Fgf10-hippo epithelial-mesenchymal crosstalk maintains and recruits lung basal stem cells. *Dev Cell*. 2017;43:48-59.e5.
24. Volckaert T, Campbell A, Dill E, Li C, Minoo P, De Langhe S. Localized Fgf10 expression is not required for lung branching morphogenesis but prevents differentiation of epithelial progenitors. *Development*. 2013;140:3731-3742.
25. Moiseenko A, Vazquez-Armendariz AI, Kheirollahi V, et al. Identification of a repair-supportive mesenchymal cell population during airway epithelial regeneration. *Cell Rep*. 2020;33:108549.

26. Yamasaki M, Miyake A, Tagashira S, Itoh N. Structure and expression of the rat mRNA encoding a novel member of the fibroblast growth factor family. *J Biol Chem*. 1996;271:15918-15921.

27. Rubin JS, Osada H, Finch PW, Taylor WG, Rudikoff S, Aaronson SA. Purification and characterization of a newly identified growth factor specific for epithelial cells. *Proc Natl Acad Sci USA*. 1989;86:802-806.

28. Francavilla C, Rigbolt KTG, Emdal KB, et al. Functional proteomics defines the molecular switch underlying FGF receptor trafficking and cellular outputs. *Mol Cell*. 2013;51:707-722.

29. Rehan VK, Torday JS. The lung alveolar lipofibroblast: an evolutionary strategy against neonatal hyperoxic lung injury. *Antioxid Redox Signal*. 2014;21:1893-1904.

30. Kruglikov IL, Scherer PE. The role of adipocytes and adipocyte-like cells in the severity of COVID-19 infections. *Obesity*. 2020;28:1187-1190.

31. Ferreira-Gomes M, Kruglov A, Durek P et al. SARS-CoV-2 in severe COVID-19 induces a TGF-beta-dominated chronic immune response that doest not target itself. *Nat Commun*. 2021;12:1961.

SUPPORTING INFORMATION

Additional supporting information may be found online in the Supporting Information section at the end of this article.

How to cite this article: Taghizadeh S, Heiner M, Vazquez-Armendariz AI, et al. Characterization in mice of the resident mesenchymal niche maintaining AT2 stem cell proliferation in homeostasis and disease. *Stem Cells*. 2021;39(10):1382–1394. https://doi.org/10.1002/stem.3423